Role of Defects on Electronic Properties in Various Mono Layer Transition Metal Dichalcogenides

Ravinder Pawar*

Department of chemistry, National Institute of Technology Warangal (NITW), Warangal, Telangana-506004, India

ABSTRACT

The chalcogen vacancy defects in various transition metal dichalcogenides (TMDCs) have been studied using density functional theory (DFT) calculation. Results reveal that (i) the dissociation energy value depends on both nature of chalcogen and transition metal, (ii) the work function depends marginally on the single or double vacancies, (iii) the defect transforms direct band gap to indirect band gap materials (i.e. the pristine materials show $K_V \rightarrow K_C$ transition whereas defective materials show $\Gamma_V \rightarrow K_C$) and (iii) the *d*-orbital of the transition metal plays a vital role in the formation of impurity band.

*E-mail: ravinder_pawar@nitw.ac.in

INTRODUCTION

Scrutiny of two-dimensional (2D) electronic materials is an emerging research area. The importance of high quality 2D materials is well known due to their interesting physics and potential applications for electronic devices.[1–9] One of the important class of 2D semiconductors and semimetals is layered transition-metal dichalcogenides (TMDCs).[4–15] From the bulk structure, these layered materials could be exfoliated into thin film to explore their exotic features for practical applications. Various methods, such as mechanical exfoliation, liquid exfoliation, hydrothermal intercalation/exfoliation, chemical vapor deposition (CVD), as well as two-step expansion and intercalation have been developed to synthesize few-layers of various TMDC nanosheets.[12, 16–19] Tremendous research efforts have been focused on the TMDCs due to their potential applications in areas such as electronic, optoelectronic, and photovoltaic devices.[7, 12, 20] The TMDCs consisting molybdenum and tungsten as metal constituent are semiconductors exhibiting band gap range from visible to the near-infrared. Similarly, chalcogenides formed with Ti, Sn, and Zr are also predicted to be semiconducting materials but little to no experimental evidence exists on their isolation in monolayer form, stability, or performance in devices.[21–25] Thus, Mo and W chalcogenides have been the most heavily investigated among the post graphene two-dimensional materials. Structure of TMDCs exhibits the metal atoms in a six fold coordination environment are hexagonally packed between two trigonal atomic layers of chalcogen atoms.[26]

The defects usually play an important role in modifying the various properties of different quasi one and two-dimensional materials. Similar to graphene, the TMDCs are also not found to be defect free.[27-34] The most commonly, the chalcogen atom missing defects or chalcogen vacancies defect found in TMDCs.[34] In this section, recent literature on the defects in various TMDC has been described. The studies on electronic structures of antisites and vacancies of m-MoS2 by atomically resolved annular dark-field scanning transmission

electron microscopy (ADF-STEM) imaging and density functional theory (DFT) calculation have been carried out to understand the electric and magnetic properties induced by these point defects.[19] Results have demonstrated that minimizing point defects, especially antisites, is paramount for electric transport applications, while controllably introduced antisites may produce atomic size local magnetic moments.[19] Zhou et al. have carried out a systematic study of intrinsic structural defects in chemical vapor phase grown monolayer MoS_2, including point defects, dislocations, grain boundaries, and edges, via direct atomic resolution imaging, and explore their energy landscape and electronic properties using first-principles calculations.[18] It can be found from their results that a rich variety of point defects and dislocation cores, distinct from those present in graphene, were observed in MoS_2.[18] It has also been reported that carrier mobility in CVD grown MoS_2 monolayers is much lower than that of mechanically exfoliated samples of the same due to the growth process imperfections and the induced structural defects in the material.[18]

Furthermore, scrutiny of charge transport of few-layer MoS_2 revealed that the defect-induced localized states found to be the responsible factor for the low-carrier-density.[35] The performance and properties of semiconductor based nano-electronic devices mainly depend on the contacts and interfaces of semiconductors.[36-37] Recent reports on tuning the on-off current ratio and the field-effect mobility of MoS_2 devices via Schottky Barrier height control and device engineering by various contact materials. However, it will be affected by the nature of defects and their concentration, since the intrinsic or interfacial defect states and work functions play a role in determining Schottky Barrier height.[38] Recently, Lee and coworkers have studied the strain-induced magnetism in single-layer various pristine and defective MoS_2. The results highlights when the tensile strain is applied, 1L-MoS_2 with vacancy becomes ferromagnetic and metallic. They also stated that the impurity bands inside

the gap play a role of seed to drive novel magnetic and electronic properties as the strain increases.[34]

Although, several reports available on the study of MoS_2 but other TMDCs are scarce. Therefore, in the present investigation a systematic attempt has been made to understand the formation of chalcogen vacancies in various TMDCs and its role on the electronic properties of these material using density functional theory (DFT) calculations. The comparative analysis has also been carried out with the properties of corresponding native (pristine) materials.

COMPUTATIONAL DETAILS

The density functional theory (DFT) calculations using the plane-wave basis set (plane-wave cutoff of 400 eV) with the projector augmented wave (PAW) method were carried out. Geometry of all pristine monolayer TMDC slab were optimized using density functional theory (DFT) based Perdew−Burke−Ernzerhof within generalized gradient approximation (PBE-GGA) method.[39-41] A Brillouin zone sampling was considered on a Gamma centered 9×9×1 grid. Geometry optimization was performed, relaxing both ions and lattices until the total energy variation was less than 10^{-6} eV. In the present investigation, significantly large (~38 Å) vacuum considered on each slab for avoiding the interaction between periodic images and to attain the appropriate approximation for the electrostatic potential in vacuum. Calculated lattice constant (a_o) for pristine MoS_2, $MoSe_2$, WS_2, and WSe_2 are 3.22, 3.37, 3.21 and 3.37 Å, respectively. Same values reported by Ding et al. defer only marginally.[42] To avoid size effects as much as possible, a 4x4 atom slab was used in the approximation for defect studies. The same geometries were used in throughout study.

Evidence from the previous studies clearly reveals PBE (GGA) significantly underestimates the energy gap. Therefore, an ultra-soft pseudo-potential description of the electron-electron interaction was used within LDA approximation for the calculating the

Kohn-Sham energy bands. An 80 Ry wave function and a 500 Ry charge density cut-off were taken into account. All calculations were conducted exploiting the both VASP and Quantum-ESPRESSO programs.[43, 44]

The chalcogen atom dissociation energy (E_{Dn}) of various TMDSs per chalcogen atom was calculated using following equations:

$$E_{Dn} = -\left(E_{\text{Prist}} - \left(E_{\text{Def}} + n * E_{\text{Chal}}\right)\right)$$

Where, E_{Prist}, E_{Def} and E_{Chal} represent the energy of pristine, defective TMDCs and energy of isolated chalcogen atom, respectively. n is number of cahlcogen vacancy in corresponding defective TMDCs. The energy of isolated chalcogen is calculated in same periodic boundary conditions with single chalcogen atom.

The work function (WF) was defined as the minimum energy which was necessary to extract an electron far from Fermi level into the vacuum level.

$$WF = V_L - E_F$$

where V_L represents the energy of vacuum level and E_F represents the energy of Fermi level. The vacuum level has been determined by the electrostatic potential in the vacuum region, and has a sufficient distance from the system in the Z direction.

RESULTS AND DISCUSSION

Geometry

The slab models considered in the present investigation are shown in **Figure 1**. The pristine slab represented as **P**, the slab with single chalcogen vacancy denoted as **D1** and slab with double chalcogen vacancy represented as **D2**. The calculated average distance between two consecutive defective sites in **D1** for MoS_2, $MoSe_2$, WS_2 and WSe_2 are 12.87, 13.48, 12.83 and 13.49 Å, respectively. Corresponding distances for **D2** are 12.87, 13.47, 12.83 and 13.48. Though, the deviation in the average distances of defective site for **D1** and **D2** is negligible but the same is significant when compared with corresponding pristine counterpart.

Therefore, it is also interesting to observe the other geometrical parameters. All important geometrical parameters of active site defined in **Scheme 1** and corresponding values are given in **Table 1**.It can be seen that the other geometrical parameters vary significantly from pristine to vacancy TMDCs.

Energies

To gain insight into the stability of the various defective materials in the present investigation energetic analysis has performed. Calculated chalcogen atom dissociation energy (E_{Dn}) for diferent materials are given in **Table 2**. It can be noticed that the dissociation energy value depends on both nature of chalcogen and transition metal. Close analysis of energetic clearly reveals that the dissociation energy the TMDCs with S atom have significantly higher energy when compared with TMDCs with Se atom. The variation may be attributed due to the high electronegativity of S atom. Furthermore, the dissociation energy of second chalcogen atom is approximately twice to the dissociation energy of first chalcogen atom.

Work function

Calculated electrostatic potential curves of different MoS_2 slabs with distance are shown in **Figure 2** (all other are given in supplementary information). As suggested by Bengtsson et al., dipole corrections have been taken into account during the electrostatic potential computation.[45] The work function has been extracted, computing the potential along the perpendicular direction to the TMDCs interface and subtracting the Fermi Level of the system to the vacuum level (as shown in **Figure 2**). The effect of the defect can be clearly observed from the electrostatic potential curves. Calculated work functions of different materials are given in Table 2. The work function values of transition metal sulfides significantly larger when compare to the same transition metal selenides. Typically, the difference value of work function for Mo is 414 meV and the same for W found to be 517 meV. Similarly, the effect of

variation of metal in same chalcogen also found from the same table. Further, the same trend is valid in the defective materials. Therefore, it is worthwhile to mention that the work function of both pristine and defective TMDCs depend on the nature of both metal and constituent chalcogen.

Single chalcogen vacancy creates two dissimilar surfaces of TMDCs thus in the present investigation the work functions of two different surfaces were considered. The work function of surface without any chalcogen vacancy represented as WF1 whereas the same with calcogen vacant site denoted as WF2 (as shown in **Table 2**). The values of both WF1 and WF2 clearly indicate that the chalcogen vacancy significantly influences the surface-electron binding property of material. In the case of MoS_2 the difference of work function of **P** and same face in **D1** is 33 meV. It can also be found from the same table that the work function difference for two different surfaces of same materials (in the case of **D1**) is only marginal. Therefore, the value of work function only marginally depends on the single and double vacancies.

Electronic structure

The pristine form of monolayer TMDCs considered in the study (MoS_2, $MoSe_2$, WS_2 and WSe_2) are semiconductors with direct band gap at K point in Brillouin zone. The calculated energy gap ($E_g = K_c - K_v$) values for pristine monolayer MoS_2, $MoSe_2$, WS_2 and WSe_2 are 1.52, 1.26, 1.63 and 1.27 eV, respectively. The same values obtained in Ding et al are deviates significantly.[42] The observed deviation attribute to the different methods used in present investigation for structural relaxation and electronic structure.

Calculated Kohn-Sham energy band structures of various TMDCs with single chalcogen vacancy along with E_g values are shown in **Figure 3**. Red bands in figure represent the bands formed due to the defect in the material. Single chalcogen vacancy converts all direct gap semiconductors to indirect gap semiconductors. The possible electron transition in defective

materials found between $\Gamma_v \rightarrow K_C$ instead $K_v \rightarrow K_C$ as found in their native structure. Furthermore, it can be seen from the same figure that the energy gap significantly decreases upon inserting single chalcogen vacancy. Calculated variation in energy gap ($\Delta E_g = E_g(\text{pristine}) - E_g(\text{defective})$) varies from 60 meV to 290 meV.

The Kohn-Sham energy band structures obtained from DFT calculation of various TMDCs with double chalcogen vacancy along with E_g values are depicted in **Figure 4**. Similar to single chalcogen vacancy TMDCs, the TMDCs with double chalcogen vacancy exhibits the indirect band gap. Calculated variation of energy gap for MoS_2, $MoSe_2$, WS_2 and WSe_2 are 380, 230, 280 and 160 eV, respectively. The decrease in band gap upon double chalcogen vacancy is higher when compare with their counter parts with single chalcogen vacancy. Therefore, it is noteworthy to mention that the trend found in energy gap is as follow: Eg (Pristine TMDCs) > Eg (TMDCs with single chalcogen vacancy) > Eg (TMDCs with double chalcogen vacancy). It is also interesting to observe that the band obtained due to defect is significantly closer to the conduction band. In the case of D2-$MoSe_2$ the band formed due to defect completely over laps the conduction band.

To gain insight in to the close understanding of the defective state formation in this study the local density of states (LDOS) evaluated for each system. Calculated LDOS of various pristine and defective MoS2 are given in **Figure 5** (other are given in supplementary information) and couture plot revealing the charge density difference ($\rho = \rho_{\text{Pristine}} - \rho_{\text{Defective}}$) from native system is shown in Figure 6. It can be seen from the figure that the density peak close to the Fermi level represents the formation of defective band. Close analysis of LDOS clearly reveals that the band formed due to defect is mainly formed from the metallic d-orbital.

CONCLUSIONS

The results obtained from the study of chalcogen vacancy defects in various transition metal dichalcogenides (TMDCs) indicate that the nature of both metal and chalcogen plays role in the dissociation energy. It can also be found from the DFT analysis that electron binding property to surface significantly influenced upon the variation of chalcogen but only have marginal effect of the number of vacancies. The introduction of defect in these TMDCs converts these materials from direct band gap to indirect band gap. The electronic transformation in pristine TMDCs favorably takes place between K_V and K_C whereas same for the defective materials found to be Γ_V and K_C. The local density of states calculation clearly reveals the role of d-orbital in the formation of impurity band.

AUTHOR INFORMATION

Corresponding Author *E-mail: ravinder_pawar@nitw.ac.in

ACKNOWLEDGMENTS

Financial support from DST-SERB is gratefully acknowledged.

REFERENCES

1. Geim, A. K.; Novoselov, K. S. The Rise of Graphene. *Nat. Mater*. **2007**, *6***,** 183–191.
2. Neto, A. H. C.; Guinea, F.; Peres, N. M. R.; Novoselov, K. S.; Geim, A. K. The Electronic Properties of Graphene. *Rev. Mod. Phys*. **2009**, 81, 109–162.
3. Liu, Y.; Wang, G.; Huang, Q.; Guo, L.; Chen, X. Structural and Electronic Properties of T Graphene: A Two-Dimensional Carbon Allotrope with Tetrarings. *Phys. Rev. Lett*. **2012**, *108*, 225505.
4. Splendiani, A.; Sun, L.; Zhang, Y.; Li, T.; Kim, J.; Chim, C.; Galli, G.; Wang, F. Emerging Photoluminescence in Monolayer MoS_2. *Nano Lett*. **2010**, *10***,** 1271–1275.
5. Yoon, Y.; Ganapathi, K.; Salahuddin, S. How Good Can Monolayer MoS_2 Transistors Be?. *Nano Lett*. **2011,** *11*, 3768–3773.
6. Castellanos-Gomez, A.;, Barkelid, M.; Goossens, A. M.; Calado, V. E.; van der Zant, H. S. J.; Steele, G. A. Laser-Thinning of MoS2: On Demand Generation of a Single-Layer Semiconductor. *Nano Lett*. **2012**, *12*, 3187–3192.
7. Novoselov, K. S.: Jiang, D.; Schedin, F.; Booth, T. J.; Khotkevich, V. V.; Morozov, S. V.; Geim, A. K. Two-dimensional atomic crystals. *Proc. Natl. Acad. Sci. U. S. A*. **2005**, *102*, 10451–10453.
8. Mak, K. F.; Lee, C.; Hone, J.; Shan, J.; Heinz, T. F. Atomically Thin MoS_2: A New Direct-Gap Semiconductor. *Phys. Rev. Lett*. **2010**, *105*, 136805.
9. Yim, C.; O'Brien, M.; McEvoy, N.; Riazimehr, S.; Schäfer-Eberwein, H.; Bablich, A.; Pawar, R.; Iannaccone, G.; Downing, C.; Fiori, G.; Lemme, M. C.; Duesberg, G. S. Heterojunction Hybrid Devices from Vapor Phase Grown MoS_2. *Sci. Rep.* **2014**, *4*, 5458.
10. Cunningham, G.; Hanlon, D.; McEvoy, N.; Duesberg, G. S.; Coleman, J. N. Large Variations in both Dark- and Photoconductivity in Nanosheet Networks as Nanomaterial is Varied from MoS_2 to WTe_2. *Nanoscale* **2015**, *7***,** 198–208.
11. Duesberg, G. S. Heterojunctions in 2D Semiconductors: A Perfect Match. *Nat. Mater.* **2014**, *13***,** 1075–1076.
12. Radisavljevic, B.; Radenovic, A.; Brivio, J.; Giacometti, V.; Kis, A. Single-Layer MoS2 Transistors. *Nat. Nanotechnol*. **2011**, *6*, 147–150.
13. Wang, H.; Yu, L.; Lee, Y. –H; Shi, Y.; Hsu, A.; Chin, M. L.; Li, L. –J.; Dubey, M.; Kong, J.; Palacios, T. Integrated Circuits Based on Bilayer MoS_2 Transistors. *Nano Lett*. **2012**, *12*, 4674–4680.

14. Radisavljevic, B.; Whitwick, M. B.; Kis, A. Small-Signal Amplifier Based on Single-Layer MoS_2. *Appl. Phys. Lett*. **2012**, *101*, 043103.
15. Lopez-Sanchez, O.; Lembke, D.; Kayci, M.; Radenovic, A.; Kis, A. Ultrasensitive Photodetectors Based on Monolayer MoS_2. *Nat. Nanotechnol*. **2013**, *8*, 497–501.
16. Coleman, J. N.; Lotya, M.; O'Neill, A.; Bergin, S. D.; King, P. J.; Khan, U.; Young, K.; Gaucher, A.; De, S.; Smith, R. J.; et al. Two-Dimensional Nanosheets Produced by Liquid Exfoliation of Layered Materials. *Science* **2011**, *331*, 568−571.
17. Lee, Y.-H.; Zhang, X.-Q.; Zhang, W.; Chang, M.-T.; Lin, C.-T.; Chang, K.-D.; Yu, Y.-C.; Wang, J. T.-W.; Chang, C.-S.; Li, L.-J.; et al. Synthesis of Large-Area MoS_2 Atomic Layers with Chemical Vapor Deposition. *Adv. Mater*. **2012**, *24*, 2320−2325.
18. Zhou, W.; Zou, X.; Najmaei, S.; Liu, Z.; Shi, Y.; Kong, J.; Lou, J.; Ajayan, P. M.; Yakobson, B. I.; Idrobo, J.-C. Intrinsic Structural Defects in Monolayer Molybdenum Disulfide. *Nano Lett*. **2013**, *13*, 2615−2622.
19. Hong J, Hu Z, Probert M, Li K, Lv D, Yang X, Gu L, Mao N, Feng Q, Xie L, Zhang J, Wu D, Zhang Z, Jin C, Ji W, Zhang X, Yuan J, Zhang Z 2015 Exploring atomic defects in molybdenum disulphide monolayers. *Nat. Comm.*, DOI: 10.1038/ncomms7293
20. Lee, C.; Li, Q.; Kalb, W.; Liu, X.-Z.; Berger, H.; Carpick, R. W.; Hone, J. Frictional Characteristics of Atomically Thin Sheets. *Science* **2010**, *328*, 76−80.
21. Zeng, Z.; Yin, Z.; Huang, X.; Li, H.; He, Q.; Lu, G.; Boey, F.; Zhang, H. Single-Layer Semiconducting Nanosheets: High-Yield Preparation and Device Fabrication. *Angew. Chem., Int. Ed*. **2011**, *50*, 11093–11097.
22. Zhu, Z.; Cheng, Y.; Schwingenschlögl, U. Topological Phase Diagrams of Bulk and Monolayer TiS_2. *Phys. Rev. Lett*. **2013**, *110*, 077202.
23. Song, H. S.; Li, S. L.; Gao, L.; Xu, Y.; Ueno, K.; Tang, J.; Cheng, Y. B.; Tsukagoshi, K. High-Performance Top-Gated Monolayer SnS_2 Field-Effect Transistors and Their Integrated Logic Circuits. *Nanoscale* **2013**, *5*, 9666–9670.
24. Zeng, Z.; Sun, T.; Zhu, J.; Huang, X.; Yin, Z.; Lu, G.; Fan, Z.; Yan, Q.; Hng, H. H.; Zhang, H. An Effective Method for the Fabrication of Few-Layer-Thick Inorganic Nanosheets. *Angew. Chem., Int. Ed*. **2012**, *51*, 9052–9056.
25. Zeng, Z.; Tan, C.; Huang, X.; Bao, S.; Zhang, H. Growth of Noble Metal Nanoparticles on Single-Layer TiS_2 and TaS_2 Nanosheets for Hydrogen Evolution *Reaction. Energy Environ. Sci*. **2014**, *7*, 797–803.

26. Enyashin, A. N.; Yadgarov, L.; Houben, L.; Popov, I.; Weidenbach, M.; Tenne, R.; Bar-Sadan, M.; Seifert, G. New Route for Stabilization of 1T-WS_2 and MoS_2 Phases. *J. Phys. Chem. C* **2011**, *115*, 24586–24591.
27. Ataca, C.; Ciraci, S. Functionalization of Single-Layer MoS2 Honeycomb Structures. *J. Phys. Chem. C* **2011**, *115*, 13303−13311.
28. Zhou, Y.; Yang, P.; Zu, H.; Gao, F.; Zu, X. Electronic Structures and Magnetic Properties of MoS_2 Nanostructures: Atomic Defects, Nanoholes, Nanodots and Antidots. *Phys. Chem. Chem. Phys*. **2013**, *15*, 10385−10394.
29. Han, S. W.; Hwang, Y. H.; Kim, S.-H.; Yun, W. S.; Lee, J. D.; Park, M. G.; Ryu, S.; Park, J. S.; Yoo, D.-H.; Yoon, S.-P.; et al. Controlling Ferromagnetic Easy Axis in a Layered MoS_2 Single Crystal. *Phys. Rev. Lett*. **2013**, *110*, 247201.
30. He, J.; Wu, K.; Sa, R.; Li, Q.; Wei, Y. Magnetic Properties of Nonmetal Atoms Absorbed Monolayers. *Appl. Phys. Lett*. **2010**, *96*, 082504.
31. Ramasubramaniam, A.; Naveh, D. Mn-Doped Monolayer MoS_2: An Atomically Thin Dilute Magnetic Semiconductor. *Phys. Rev. B* **2013**, *87*, 195201.
32. Cheng, Y. C.; Zhu, Z. Y.; Mi, W. B.; Guo, Z. B.; Schwingenschlögl, U. Prediction of Two-Dimensional Diluted Magnetic Semiconductors: Doped Monolayer MoS_2 Systems. *Phys. Rev. B* **2013**, *87*, 100401(R).
33. Yun, W. S.; Lee, J. D. Unexpected Strong Magnetism of Cu Doped Single-Layer MoS2 and Its Origin. *Phys. Chem. Chem. Phys*. **2014**, *16*, 8990−8996.
34. Yun, W. S.; Lee, J. D. Strain-Induced Magnetism in Single-Layer MoS_2: Origin and Manipulation. *J. Phys. Chem. C* **2015**, *119*, 2822–2827
35. Qiu, H.; Xu, T.; Wang, Z.; Ren, W.; Nan, H.; Ni, Z.; Chen, Q.; Yuan, S.; Miao, F.; Song, F.; Long, G.; Shi, Y.; Sun, Y.; Wang, J.; Wang, X. Hopping Transport Through Defect-Induced Localized States in Molybdenum Disulphide. *Nat. Comm*. **2013**, *4*, 2642
36. Shih, C-. J.; Wang, Q. H.; Son, Y.; Jin, Z.; Blankschtein, D.; Strano, M. S. Tuning On–Off Current Ratio and Field-Effect Mobility in a MoS_2–Graphene Heterostructure via Schottky Barrier Modulation. *ACS Nano* **2014**, *8*, 5790–5798.
37. Chen, J-. R.; Odenthal, P. M.; Swartz, A. G.; Floyd, G. C.; Wen, H.; Luo, K. Y.; Kawakami, R. K. Control of Schottky Barriers in Single Layer MoS_2 Transistors with Ferromagnetic Contacts. *Nano Lett*. **2013**, *13*, 3106–3110.

38. Monch, W. Valence-Band Offsets and Schottky Barrier Heights of Layered Semiconductors Explained by Interface-Induced Gap States. *Appl. Phys. Lett*. **1998**, *72*, 1899–901
39. Perdew, J. P.; Burke, K.; Ernzerhof, M. Generalized Gradient Approximation Made Simple. *Phys. Rev. Lett*. **1996**, *77*, 3865−3868.
40. Blöchl, P. E. Projector Augmented-Wave Method. *Phys. Rev. B* **1994**, *50*, 17953−17979.
41. Kresse, G.; Joubert, D. From Ultrasoft Pseudopotentials to The Projector Augmented-Wave Method. *Phys. Rev. B* **1999**, *59*, 1758−1775.
42. Ding, Y.; Wangb, Y.; Ni, J.; Shi, L.; Shi, S.; Tang, W. First Principles Study of Structural, Vibrational and Electronicproperties of Graphene-Like MX_2 (M=Mo, Nb,W,Ta; X=S, Se,Te) Monolayers. *Physica B* **2011**, *406*, 2254–2260.
43. Kresse, G.; Hafner, J. Ab initio Molecular Dynamics for Liquid Metals. *Phys. Rev. B* **1993**, *47*, 558−561(R).
44. Giannozzi, P. Baroni, S. Bonini, N et al. QUANTUM ESPRESSO: a modular and open-source software project for quantum simulations of materials. J. *Phys.: Condens. Matter* **2009**, *21*, 395502.
45. Bengtsson, L. Dipole correction for surface supercell calculations. *Phys. Rev. B* **1999**, *59*, 12301–12304.

Scheme 1: **Schematic Presentation of Active Site Geometry of Defective Transition Metal Dichalcogenide (TMDC) Along with Important Geometrical Parameters Discussed in Text (D1 And D2 Represents TMDCS with Single Chalcogen And Double Chalcogen Vacancies)**

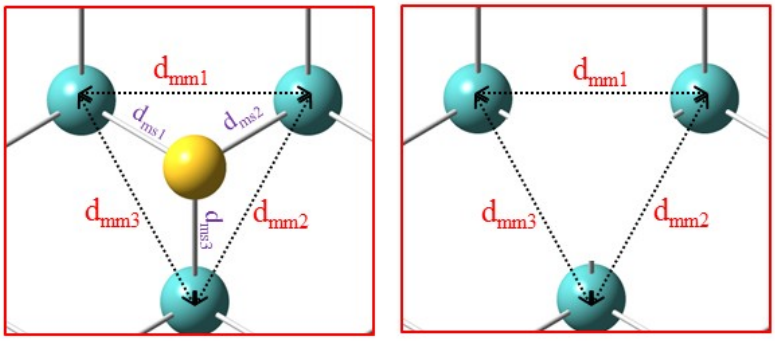

Defective1 (D1) Defective2 (D2)

Table 1. **Calculated Geometrical Parameters of Active Site in P, D1 and D2**

	d_{mm1}	d_{mm2}	d_{mm3}	d_{ms1}	d_{ms1}	d_{ms1}	
MoS_2	2.38 (2.42)	2.38	2.38	3.14 (3.22)	3.14	3.14	**D1**
$MoSe_2$	2.51 (2.55)	2.51	2.51	3.25 (3.37)	3.25	3.25	
WS_2	2.40 (2.42)	2.40	2.39	3.08 (3.21)	3.08	3.08	
WSe_2	2.53 (2.56)			3.16 (3.37)			
MoS_2	-	-	-	2.92	2.92	2.92	**D2**
$MoSe_2$	-	-	-	2.90	2.90	2.90	
WS_2	-	-	-	2.88	2.88	2.88	
WSe_2	-	-	-	2.86	2.86	2.86	

All the values are in Å and the values in parenthesis are for **P**

Table 2: **Calculated Chalcogen Atom Dissociation Energy (E_{dn}) Per Chalcogen Atom for Various Defective Materials**

System	E_{D1} (eV)	E_{D2} (eV)
MoS_2	4.941	9.926
$MoSe_2$	4.281	8.333
WS_2	5.073	9.992
WSe_2	4.423	8.367

Table 3: **Schematic Representation of the Plane from Which WF Measured and Calculated Work Functions For Various Defective Materials**

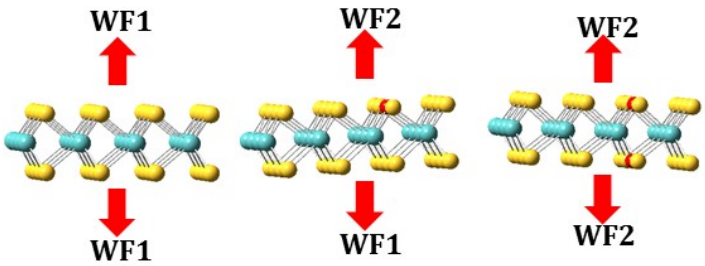

System	P		D1		D2	
	WF1	**WF2**	**WF1**	**WF2**	**WF1**	**WF2**
MoS_2	5.233		5.266	5.267		5.273
$MoSe_2$	4.819		4.850	4.870		4.879
WS_2	5.942		5.844	5.875		5.873
WSe_2	5.425		5.371	5.412		5.438

All the values are in eV

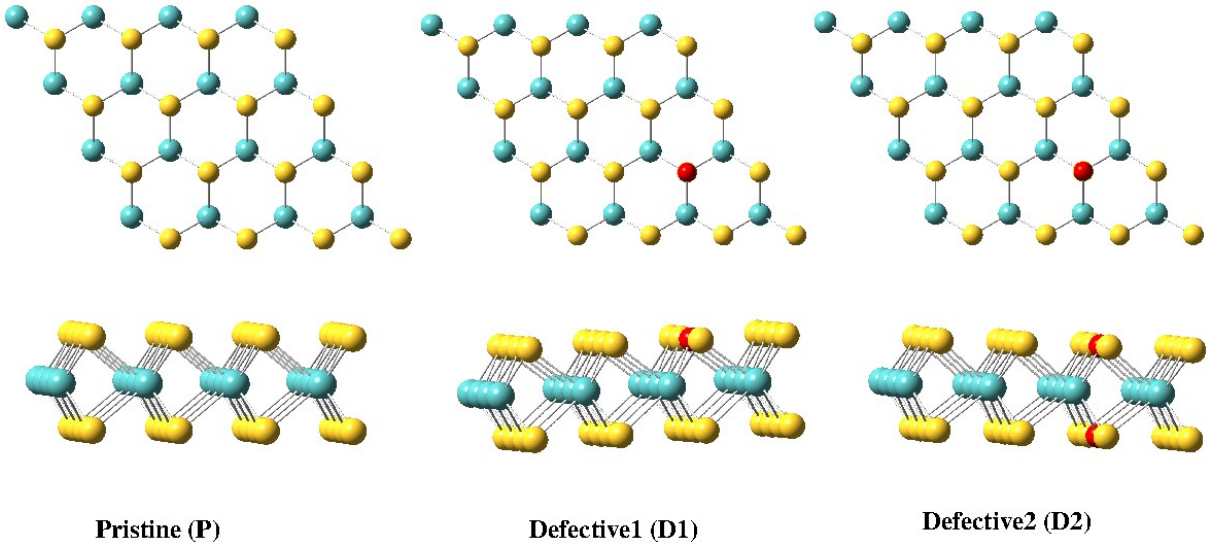

Figure 1: Model 4X4 TMDCs.

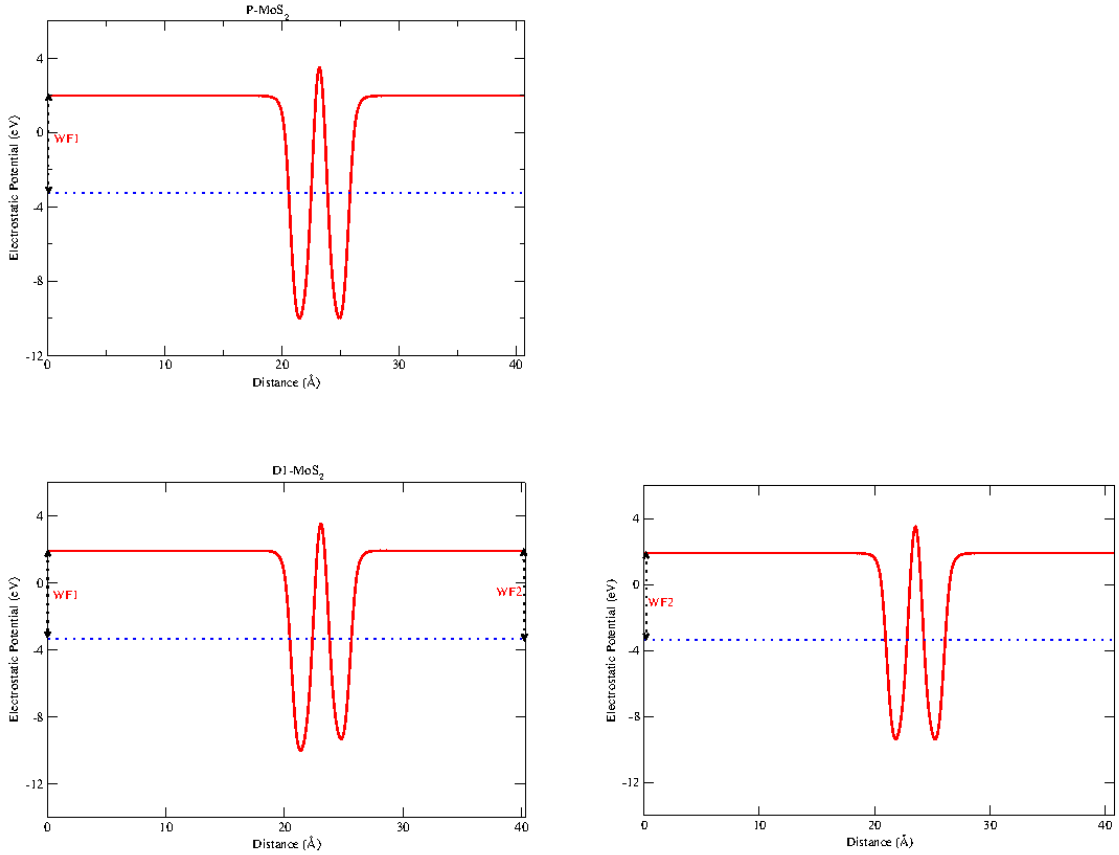

Figure 2: Electrostatic potential of pristine and defective MoS_2 slab obtained from DFT calculation.

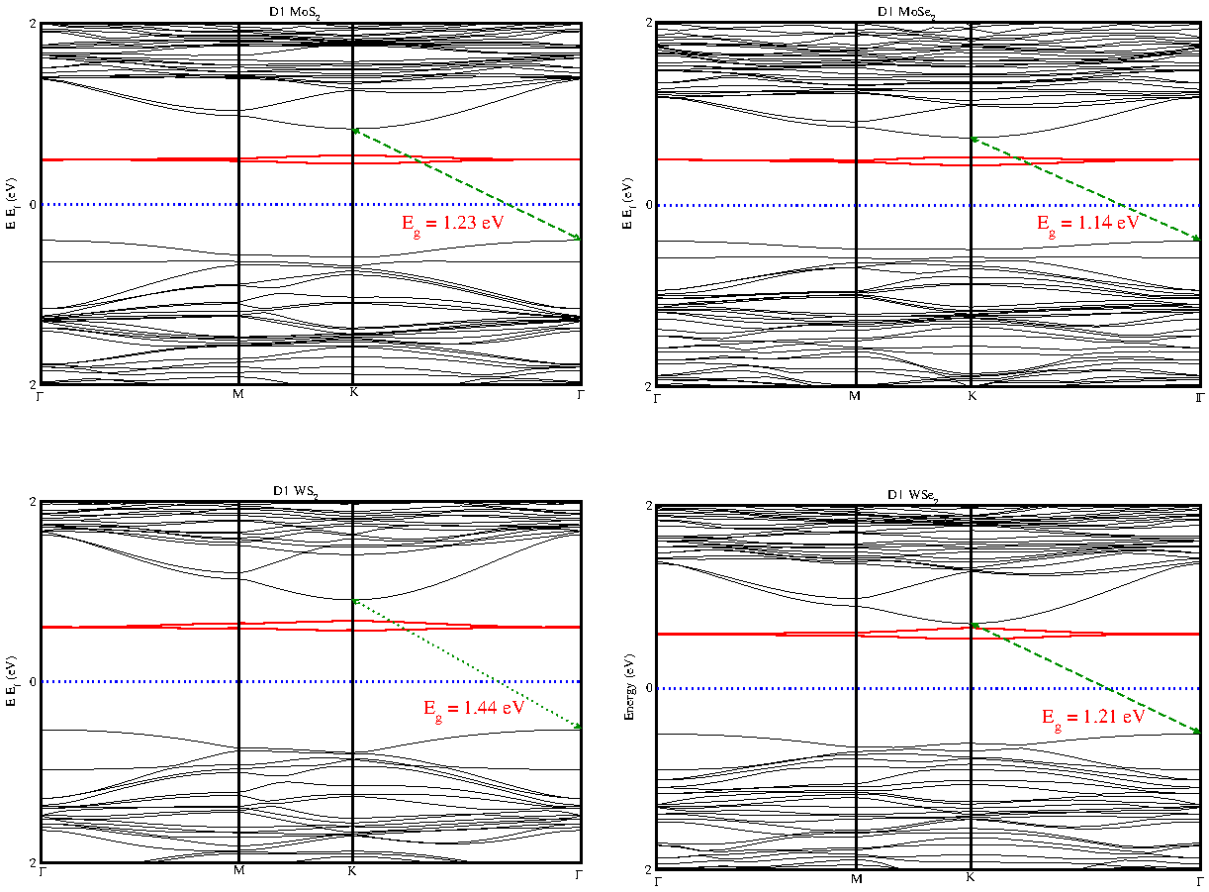

Figure 3: KS Band structure of various TMDCs with single chalcogen vacancy calculated using LDA approximation

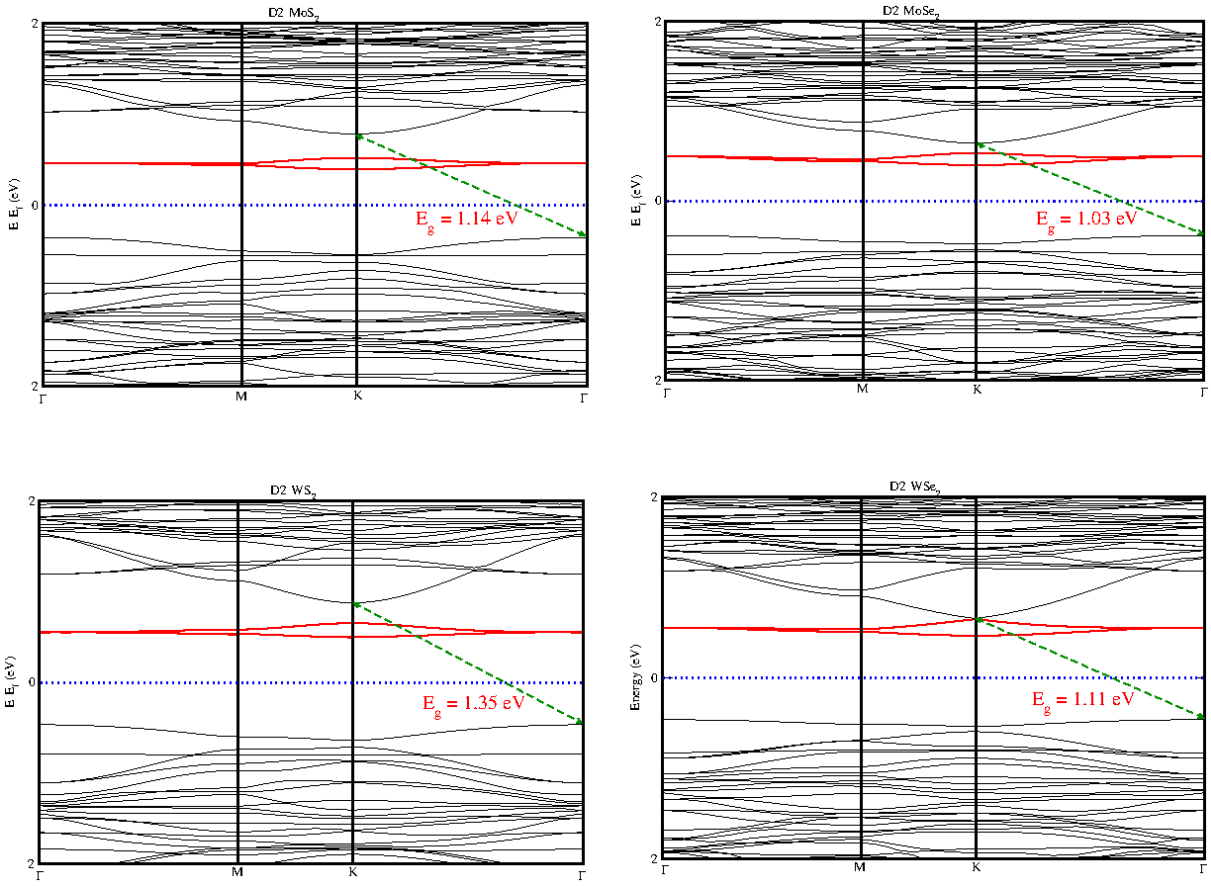

Figure 4: KS Band structure of various TMDCs with double chalcogen vacancy calculated using LDA approximation

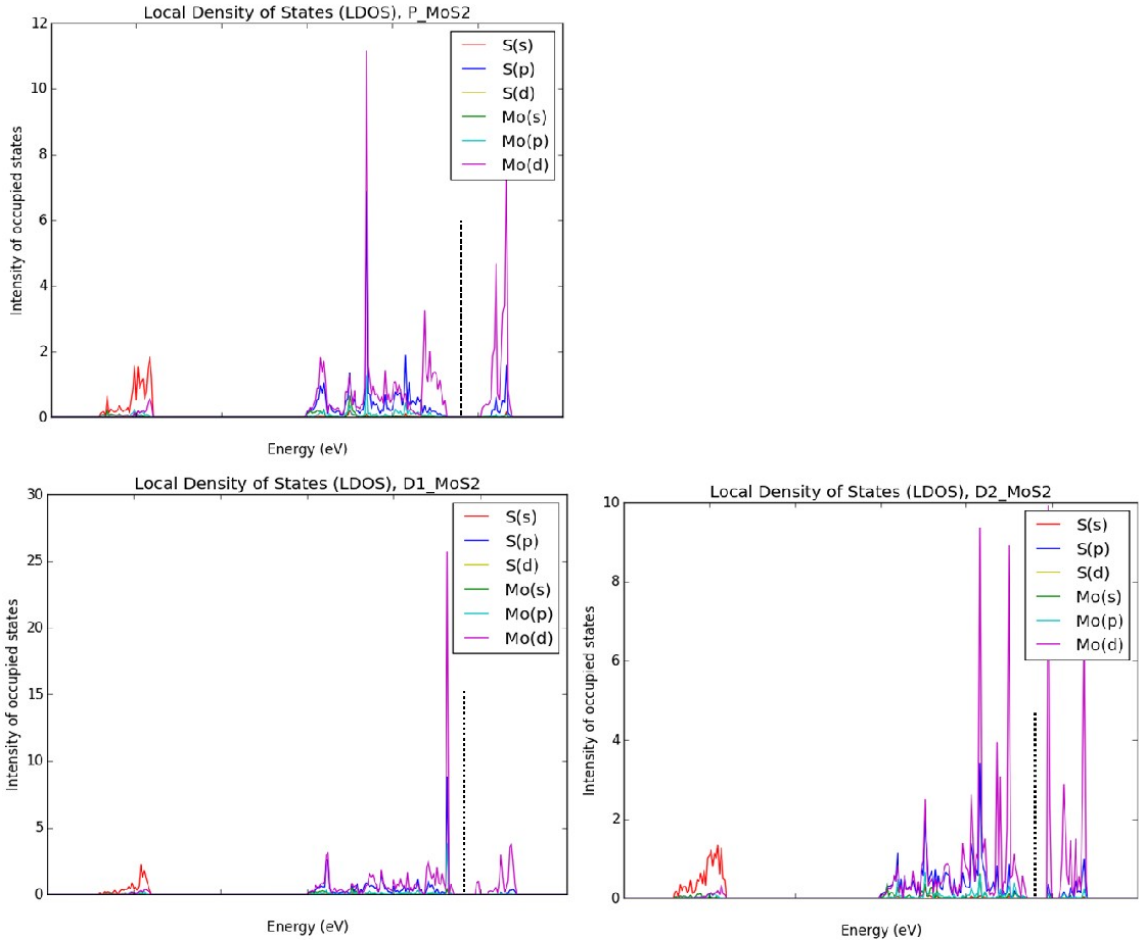

Figure 5: Local density of states of pristine, single S vacancy, and double S vacancy MoS_2 (vertical black dotted line represents the Fermi level).

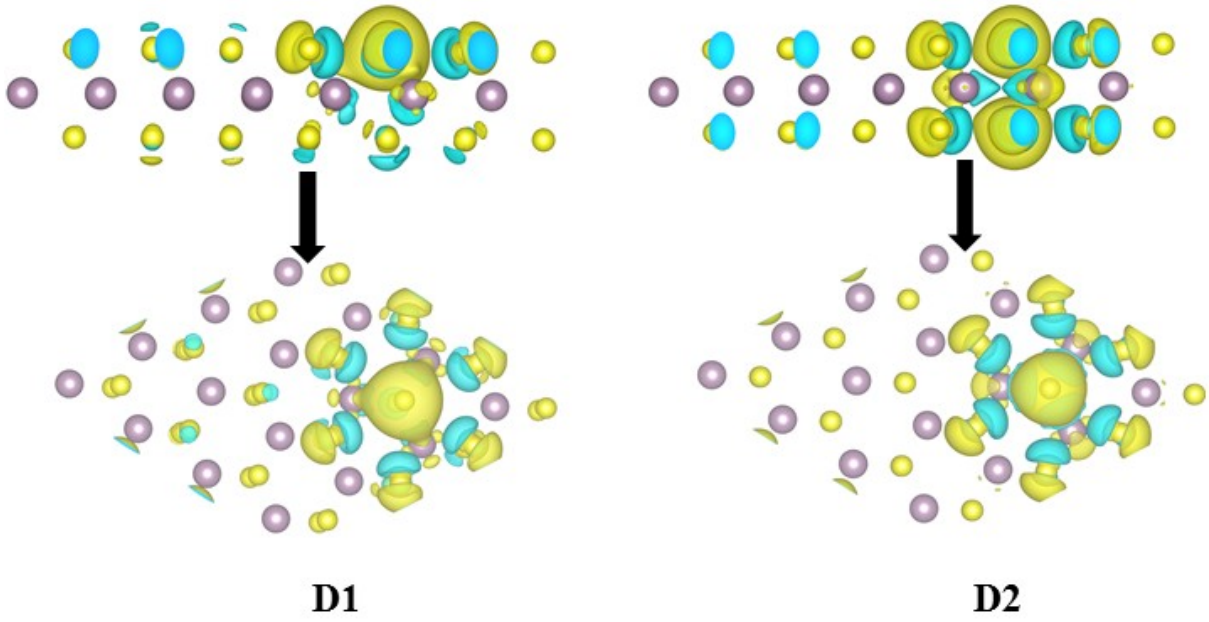

Figure 6: Calculated charge density difference of single S vacancy and double S vacancy MoS_2 with respect to pristine MoS_2.